05,08

The effect of van Hove singularities on spin pumping in the magnonic crystal/normal metal structure

© S.L. Vysotskii[1,2], Yu.V. Nikulin[1,2], G.M. Dudko[1], V.K. Sakharov[1,2], A.V. Kozhevnikov[1], M.E. Seleznev[1,2], Yu.V. Khivintsev[1,2], A.G. Khitun[3], S.A. Nikitov[4], Yu.A. Filimonov[1,2,5,¶]

[1] Saratov Branch, Kotel'nikov Institute of Radio Engineering and Electronics, Russian Academy of Sciences, Saratov, Russia
[2] Saratov National Research State University, Saratov, Russia
[3] Department of Electrical and Computer Engineering, University of California–Riverside, Riverside, California, USA 92521
[4] Kotelnikov Institute of Radio Engineering and Electronics, Russian Academy of Sciences, Moscow, Russia
[5] Yuri Gagarin State Technical University of Saratov, Saratov, Russia

¶ E-mail: yuri.a.filimonov@gmail.com

Received April 18, 2024
Revised April 18, 2024
Accepted May 8, 2024

Using the inverse spin Hall effect, spin pumping by magnetostatic backward volume waves (MSBVW) in a structure based on a magnonic crystal from an yttrium-iron garnet film and a Pt microstrip has been studied. A resonant increase in the EMF signal at the frequencies of Bragg resonances (BR) was detected, which reflects an increase in the efficiency of spin pumping. The resonant amplification of spin pumping is explained by an increase in the efficiency of electron-magnon scattering due to the formation of dispersion regions with a high density of van Hove singularities in the MSBVW spectrum at BR frequencies.

Keywords: spin pumping, spin waves, density of states, magnonic crystal, structures yttrium-iron garnet/platinum (YIG/Pt).

DOI: 10.61011/PSS.2024.07.58972.38HH

1. Introduction

Magnon insulator spintronics — is an area of spintronics related to data processing technologies and devices where spin current is applied flowing in the magnet insulator (MI) materials by means of spin waves (SW) (or magnons) [1–3]. In MI film based and normal metal (NM) based structures [4–13] the exchange interaction of conductance electrons with the spins of magnet ions localized on the MI/NM interface and the spin-orbit interaction result in the spin-dependent electron-magnon scattering and generation of a spin current through the interface. The spin current J_s, transferred through a unit surface area is defined as a difference of the interface reflectivity relative to the electrons with opposite spin orientation in the electron-magnon scattering [14]. The value J_s is proportional to the number of scattering channels defined by the number of magnetic ions exchange-coupled with NM electrons on MI surface and is defined by selecting the process parameters influencing the roughness, elemental composition and microstructure of the interface [15–17]. On the other hand, J_s represents an intensity of the electron-magnon scattering processes in each of the channels and is defined by parameters of the interacting electron and magnon sub-systems, including the electron density of states (DS) at Fermi level g_{el} and the magnon DS $g(\omega)$ depending on frequency (ω) in SW spectrum of MI/NM structure [18]:

$$J_s \sim \int g_{el} \cdot g(\omega) d\omega. \quad (1)$$

From (1) it follows that for efficient generation of J_s it is necessary to develop structures and find conditions which could provide the existence of Van Hove singularities (VHS) on MI/NM interface [19] for both, the electrons ($g_{el} \to \infty$), and the magnons ($g(\omega) \to \infty$).

Recently it has been demonstrated that the new conducting layers placed between the films of yttrium-iron garnet ($Y_3Fe_5O_{12}$ (YIG)) and platinum (Pt) may result in higher DS of electrons g_{el} at the interface and this will also be accompanied with increase of J_s [20,21] and higher levels of EMF signals generated due to the inverse spin Hall effect (ISHE) V_{ISHE} ($V_{\mathrm{ISHE}} \sim J_s$) [20]. It was also demonstrated that by means of electric field the electrons density of states at Fermi level can be controlled in Pt film [22,23].

To search the conditions of efficient spin pumping by coherent SW it is convenient to use the match [19] of VHS frequencies in the film spectrum where SW group velocity is $V_g = \nabla_{\mathbf{k}}\omega(\mathbf{k}) \to 0$, where $\omega = \omega(\mathbf{k})$ — SW dispersion law, $\mathbf{k}$ — wave vector in the film plane. A typical geometry of the experiment for spin pumping suggests that the outer

magnetic field **H** lies in the plane of structure [4–13]. The spectrum of dipole magnetostatic waves (MSW) relative to the magnetized film YIG consists of a magnetostatic surface (MSSW) and backward volume waves (MSBVW) [24]. The MSBVW with a wave vector $\mathbf{k} \parallel \mathbf{H}$ cover the frequency band $[\omega_H, \omega_0]$, where $\omega_0 = \sqrt{\omega_H^2 + \omega_H \omega_m}$, $\omega_H = \gamma H$, $\omega_m = \gamma 4\pi M$, γ and $4\pi M$ are the gyromagnetic ratio and magnetization of YIG, respectively. MSSW at $\mathbf{k} \perp \mathbf{H}$ occupy the frequency band $[\omega_0, \omega_s]$, where $\omega_s = \omega_H + \omega_m/2$. The frequency dependences of DS $g(\omega)$ within the spectrum of MSBVW and MSSW were described in paper [24] and for the MSBVW, which is of interest to us, the dependence $g(\omega)$ can be expressed as follows:

$$g(\omega) = \frac{\omega \omega_m}{\omega_H \sqrt{\omega_0^2 - \omega^2}}. \qquad (2)$$

The density of states $g(\omega)$ within MSBVW spectrum has singularity at a frequency of ω_0 ($g(\omega_0) \to \infty$) matching the frequency of homogeneous ferromagnetic resonance. The pole at $\omega \to \omega_0$ of function $g(\omega)$ represents a frequency degeneracy of dipole MSBVW with $\mathbf{k} \perp \mathbf{H}$. Experiments for spin pumping in YIG/Pt structures by dipole MSBVW showed that EMF frequency dependence $V_{\mathrm{ISHE}}(f)$ ($f = \frac{\omega}{2\pi}$) correlates with expression (2) and EMF reaches maximal values at frequencies $f \approx f_0$ [25,26].

The purpose of this paper is to show that under spin pumping by MSBVW in a structure composed of YIG film with a periodic grating consisting of grooves (magnonic crystal (MC)) etched on its surface, and contacting with Pt microstrip, the dependence $V_{\mathrm{ISHE}}(f)$ may have additional maximums to appear at Bragg resonance (BR) frequencies f_B.

It should be noted that MSBVW propagation in YIG-film based magnonic crystal was reviewed in papers [27–30]. It was found that formation of a grating with period Λ on the surface of YIG film at frequencies f_B will lead to appearance of signal rejection bands in the MSBVW transmission spectrum [27–30], and in dispersion law $k(f)$ — appearance of abnormal dispersion areas [30]. These peculiarities in MSBVW propagation demonstrate the existence of band gaps in MC spectrum at frequencies f_B. At that, on the edges of the band gap the dispersion areas with $V_g \to 0$ [31–33] were formed which was a characteristic attribute of van Hove singularities (VHS). Our purpose was to demonstrate that in MC-Pt structure the growth of efficient spin pumping at frequencies f_B is associated with the DS growth in the frequencies band corresponding to the band gap.

2. Experiment description

The experiments were carried out for a structure based on YIG film $d = 7.4\,\mu$m thick, effective magnetization of $4\pi M = 1860$ G and 2D-dimensions of 6 mm × 10 mm. Using photolithography and ion etching methods a grating

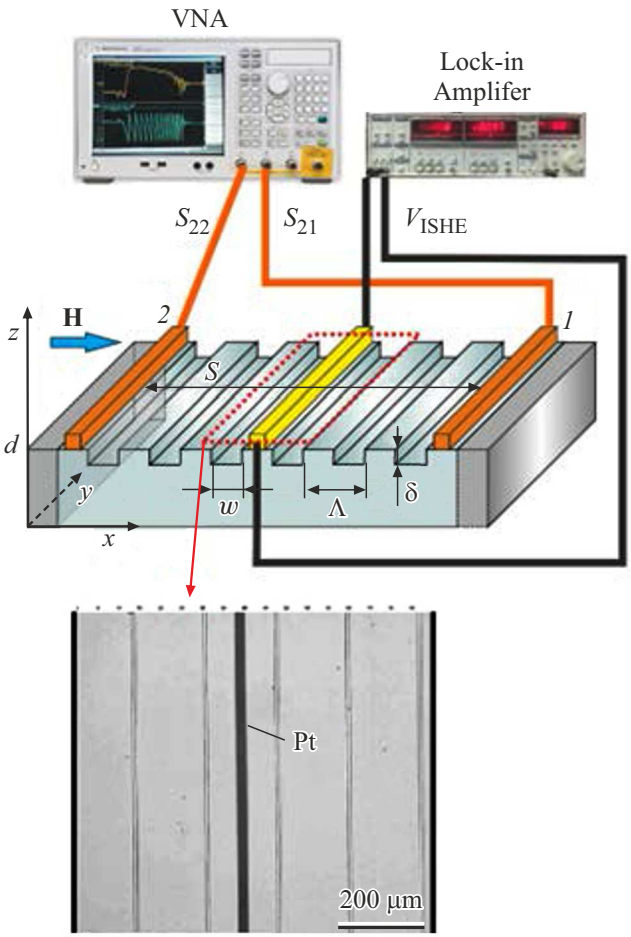

Figure 1. Scheme of experiment and MC/Pt structure. An insert image in Figure 1 shows a photo of MC surface with Platinum microstrip. Numbers *1* and *2* show SW antennas connected to the vector network analyzer's outputs.

with grooves $w = 10\,\mu$m wide, $\delta = 0.2\,\mu$m deep, 6 mm long and period $\Lambda = 170\,\mu$m was formed across the entire film surface. After that, using photolithography and ion etching methods on the surface of MC crystal a Pt microstrip 4 nm thick, 25 μm wide, 6 mm long was fabricated, see Figure 1. The MC-Pt structure was placed on the copper strip antennas 5 mm long and $w = 40\,\mu$m wide. At that the grooves were parallel to the spin waves (SW) antennas. The distance between antennas was $S = 5$ mm. The contacts to Pt microstrip were fabricated using a current-conducting paste. The structure was placed in the electromagnet gap, the field **H** of which was oriented perpendicular to the SW antennas and etched grooves, thus corresponding the MSBVW geometry.

MSBVW characteristics were measured using a vector network analyzer. The transmission spectra $S_{21}(f)$ and reflectance $S_{22}(f)$ at the incident power $P_{\mathrm{in}} = -20$ dBm were measured. The frequency dependences of EMF $V_{\mathrm{ISHE}}(f)$ were measured under modulation of the incident microwave power $P_{\mathrm{in}} = 7$ dBm with frequency of 11 kHz.

Micromagnetic simulation of MSBVW propagation was carried out using a shareware program Object Oriented Micromagnetic Framework (OOMMF) [34], and post-processing of the obtained data was executed similarly to [35]. A periodic structure with parameters identical to the experimental ones was taken in the calculations. Exchange stiffness was taken $A_{ex} = 3.5 \cdot 10^{-7}$ erg/cm and SW attenuation parameter — $\alpha = 10^{-5}$. The length of the sample was taken as 64 grating periods and was 10.880 mm. The cell size was $dx \times dy \times dz = 1\,\mu\text{m} \times 1\,\mu\text{m} \times 0.2\,\mu\text{m}$. Periodic boundary conditions were applied along the axis Oy. MSBVW were excited by a field pulse directed along the axis Oz:

$$h_{in} = A \cdot sinc(2\pi f_c[t - t_0]), \tag{3}$$

where $A = 100$ A/m — pulse amplitude; $f_c = 5$ GHz — maximal possible frequency of MSBVW excited by pulse (3); t — time; $t_0 = 50$ ns — time delay. This pulse was applied to the film region $\xi = 2\,\mu$m wide, located in the center of the sample ($x_{in} = 5440\,\mu$m) considered as an input antenna. The film area $\xi = 2\,\mu$m wide located at $x_{out} = 2720\,\mu$m was used as an output antenna.

The obtained distributions $4\pi M(x, y, z, t_i)$ across the entire structure and an averaged signal (full field) under input antenna $h_{in}(t_i)$ and output antennas $h_{out}(t_i)$ remained the same every $t_i = 100$ ps during 1 μs. Further, to plot maps of the dispersion characteristics $f = f(k)$ the two-dimensional Fourier transformation in time and space from the set $4\pi M(x, t_i)$ (with averaging on y and z) was used.

To analyze the MSBVW propagation in the structures shown in Figure 1 the amplitude-frequency response characteristics (AFR) of „delay lines“ formed by the „input“ (*2*) and „output“ (*1*) antennas were calculated. At that, the AFR $S_{12}(f)$ was calculated as [36]:

$$S_{12} = 20\,\text{lg}(\text{FFT}[h_{out}]/\text{FFT}[h_{in}]), \tag{4}$$

where $\text{FFT}[h_{in}]$ and $\text{FFT}[h_{out}]$ — amplitudes of Fourier transformation from time $h_{in}(t)$ and $h_{out}(t)$, respectively.

3. Experimental results and discussion

Figure 2 shows the results of measurements of frequency dependencies of MSBVW transmission spectrum $S_{12}(f)$ and reflectance ratio $S_{22}(f)$ of the structure and EMF $V_{ISHE}(f)$ when the bias field was equal $H = 620$ Oe. It can be seen that in dependencies $S_{12}(f)$ and $S_{22}(f)$ the resonance singularity is observed that was absent in the initial YIG film, see curves *1* and *2* in Figure 2, *a, b*. For better illustration the frequencies of resonance singularities are highlighted by vertical dotted lines in Figure 2. The resonance singularities corresponding to frequencies $f_{B1} \approx 3355$; $f_{B2} \approx 3275$; $f_{B3} \approx 3198$; $f_{B4} \approx 3130$ MHz and wave vectors $k_{B1} \approx 184$ $k_{B2} \approx 368$; $k_{B3} \approx 550$; $k_{B4} \approx 736\,\text{cm}^{-1}$ are marked by asterisks. The

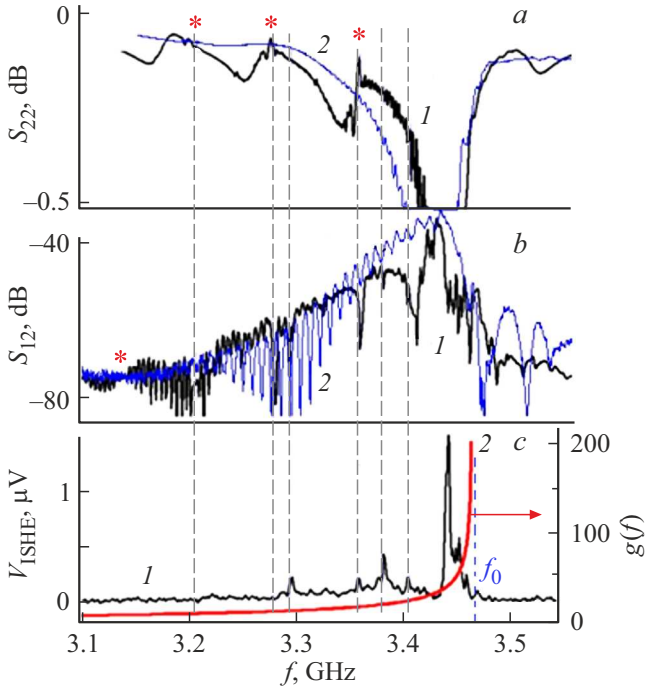

Figure 2. Frequency dependences: *a*) reflection coefficient $S_{22}(f)$ in the magnonic crystal (curve *1*) and initial YIG film(curve *2*); *b*) MSBVW transmission coefficient $S_{12}(f)$ in MC (*1*) and YIG film (*2*); *c*) EMF $V_{ISHE}(f)$ — curve *1* and density of states analysis $g(f)$ in MSBVW spectrum in YIG film as per formula (2) — curve *2*. Magnetic field $H = 620$ Oe. Position of frequency f_0 is shown in Figure 2, *c* as a vertical dotted line. The asterisks denote the BR frequencies for the fundamental mode of the MSBVW.

obtained values k_{Bn} comply with the Bragg resonance condition:

$$\mathbf{k}^+ + \mathbf{k}^- = n\mathbf{Q}, \tag{5}$$

$\mathbf{k}^+$ and $\mathbf{k}^-$ — wave vectors of the incident and reflected waves, $\mathbf{Q} = \frac{2\pi}{\Lambda}\mathbf{e}$ — wave vector of grating, $\mathbf{e}$ — unit vector oriented along the grating axis, n — order of Bragg reflection.

In frequency dependence of EMF $V_{ISHE}(f)$ at frequencies $f > 3.2$ GHz the specified resonance singularities in $S_{12}(f)$ and $S_{22}(f)$ may be comparable with the resonance peaks. Amplitude of resonance peaks depending on $V_{ISHE}(f)$ changes in the non-monotonous way with the MSBVW frequency. EMF signal at frequencies $f < 3.2$ GHz drops down to the noise level ~ 10 nV, which may be associated here with low efficiency of MSBVW excitation by antennas applied, as well as fast decrease of DS within MSBVW spectrum, see curve *2* in Figure 2, *c*. The singularities identified in dependencies $S_{12}(f)$, $S_{22}(f)$ and $V_{ISHE}(f)$ remained the same during variation of the bias field, whereas the frequencies at which they were observed were displaced together with the MSBVW excitation band.

To find the mechanism of maximums formation in dependence $V_{ISHE}(f)$ let's see the results of micro-magnetic

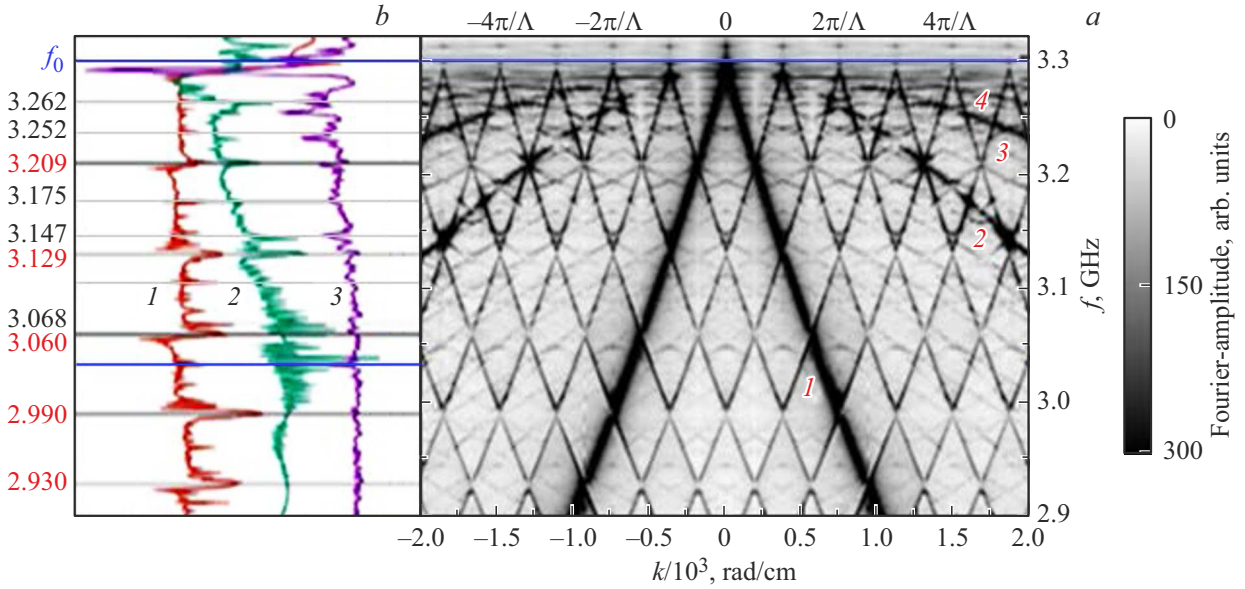

Figure 3. (a) Results of micro-magnetic simulation of MSBVW spectrum in YIG film magnonic crystal (MC) having the following parameters $d = 7.4\,\mu$m, $4\pi M = 1850$ G, exchange hardness — $A_{ex} = 3.5 \cdot 10^{-7}$ erg/cm, SW attenuation — $\alpha = 10^{-5}$, width of grooves $w = 10\,\mu$m, depth $\delta = 0.2\,\mu$m, period $\Lambda = 170\,\mu$m, length 10.88 mm. Magnetic field $H = 590$ Oe. Digits *1–4* show the numbers of the most intensive modes of MSBVW, the dispersion curves of which correspond to initial YIG film. (b) Digits *1* and *2* denote, respectively, frequency dependence from expression (4) and experimental frequency dependence of MSBVW transmission characteristic $S_{12}(f)$. Curve *3* experimental dependence of EMF $V_{\text{ISHE}}(f)$. Horizontal lines indicating the frequency (GHz) of MSBVW on curves *1–3* illustrate compliance of calculated and empirically identified resonance singularities with the Bragg resonance frequencies, for various MSBVW in Figure 3, a.

simulation of spectrum $f(k)$ and calculation using (4) of the frequency dependence of transmission spectrum $S_{12}(f)$ of MSBVW in MC, as shown in Figure 3, a and b, respectively. Figure 3, b apart from the calculated frequency dependence $S_{12}(f)$, shown in curve *1*, illustrates the experimental dependencies $S_{12}(f)$ and $V_{\text{ISHE}}(f)$ as curves *2* and *3*, respectively. The experimental dependencies $S_{12}(f)$ and $V_{\text{ISHE}}(f)$ were displaced down by 15 MHz, to include the highest number of resonance singularity frequencies. It can be seen that positions of most of the resonance singularities of calculated and experimental dependencies are matching, which is illustrated by horizontal lines in Figure 3, b.

The spectrum of MSBVW in MC as seen in Figure 3, a is characterized by a variety of Braggs resonances. Practically for every resonance singularity in the calculated dependence $S_{12}(f)$, shown as curve *1* in Figure 3, b some Bragg resonance can match in the spectrum as illustrated in Figure 3, a. The resonance-like oscillations at frequencies $f_{B1} \approx 3.209$; $f_{B2} \approx 3.129$; $f_{B3} \approx 3.06$; $f_{B4} \approx 2.99$ and $f_{B5} \approx 2.93$ GHz have resonances of fundamental mode (m = 1) of MSBVW matching to them. Resonance singularities on curve *1* (Figure 3, b) at frequencies $f_0 > f > f_{B1}$ correspond to BR of MSBVW modes with numbers m = 2, 3, 4, as well as resonances of these modes with the fundamental mode m = 1. The selected parameters of 3D grid and length of time realization do not allow to get sufficient spectrum resolution at frequencies $f_0 > f > f_{B1}$. However, as can be seen from spectrum in Figure 3, a we may make a conclusion that near frequency f_0 the band gaps in the spectrum at BR frequencies may form a wide absorption band in transmission spectrum. Another singularity of MC spectrum shall also be emphasized as seen in Figure 3, a, which looks like an „insert“ BR. This singularity is most clearly observed for BR at frequency $f_{B2} \approx 3.129$ GHz, where the fundamental mode BR area m = 1 the modes m = 3 are involved. At that, the band gaps being formed are local.

In general, looking at the MSBVW-in-MC spectrum we may suggest that dispersion areas are formed in the band gaps, where $V_g \to 0$ and where DS growth in spectrum can be expected, which will result in higher efficiency of spin pumping by the travelling MSBVW. Dependencies $V_{\text{ISHE}}(f)$ in Figure 2, c and Figure 3, b demonstrate a resonance growth of EMF at BR frequencies. At that, the amplitude of resonance peaks of EMF at frequencies f_{B1} and f_{B2}, corresponding to BR of fundamental mode of MSBVW m = 1, is sufficiently lower than peaks of amplitude at frequencies $f > f_{B1}$, see curve *3* in Figure 3, b and curve *1* in Figure 2, c. This singularity can be explained by a large group velocity of mode m = 1 compared to the modes with numbers m $\geq$ 2, which for BR with modes m $\geq$ 2 leads to broadening of a dispersion area with low group velocity. As a result the density of states in the vicinity of such BR becomes higher than for BR of the fundamental mode.

Now let's discuss the MSBVW propagation at frequencies f_{B1} and f_{B2}, which is because the BR of the mode

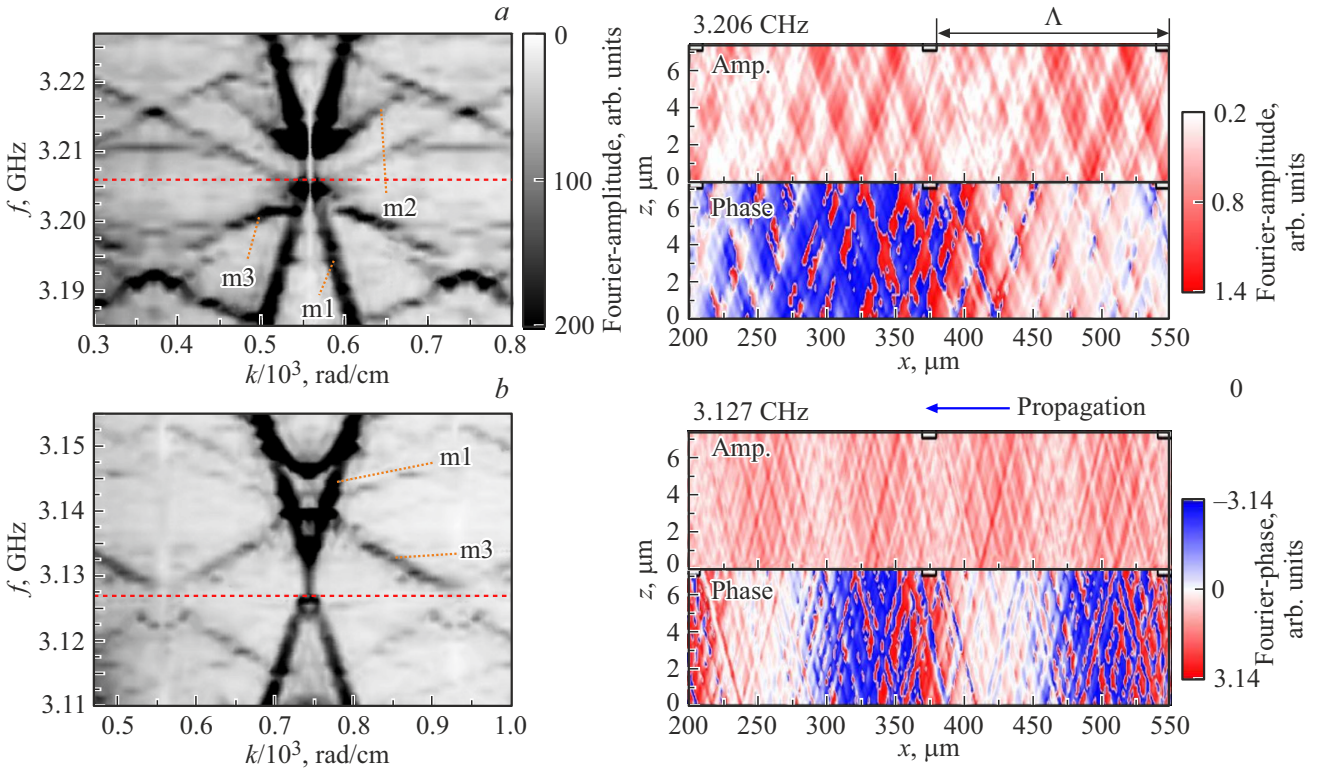

Figure 4. Charts of MSBVW amplitude and magnetization phase distribution in MC at BR frequencies with $f_{B1} \approx 3.206$ GHz (Figure 4, *a*) and $f_{B2} \approx 3.127$ GHz (Figure 4, *b*). A film area 350 μm long located 1.52 mm away from the input antenna is shown. MSBVW propagation orientation along *Ox* axis is shown with arrow. The insert windows on the left illustrate the MSBVW spectrum areas in MC as shown in Figure 3, *a*. The horizontal dotted line in the insert windows indicates position of frequencies $f_{B1} \approx 3.206$ GHz and $f_{B2} \approx 3.127$ GHz. Indices m1, m2, m3 designate the numbers of MSBVW modes.

m = 1 with the modes of other numbers m. In this case, the frequencies band corresponding to the band gap at BR mode frequency m = 1, may include the modes of MSBVW m ≥ 2 formed by Bragg reflections of $|n| \geq 3$ order. Figure 4 shows micro-magnetic simulation of Furrier distribution of MSBVW magnetization amplitudes on a 350 μm long film area 1.52 mm away from the excitation antenna for BR frequencies $f_{B1} \approx 3.206$ GHz (Figure 4, *a*) and $f_{B2} \approx 3.127$ GHz (Figure 4, *b*). Here we can see, that MSBVW magnetization amplitude decreases in direction of propagation shown by arrow in Figure 4. The distribution of amplitude and phase in Figure 4, *a* demonstrates that distribution nature is mainly defined by MSBVW modes with numbers m1 and m2. For BR at frequency $f_{B2} \approx 3.127$ GHz the nature of amplitude and phase distribution is determined by modes m = 1 and m = 3, see Figure 4, *b*.

It shall be noted that time realization $t = 1\,\mu$s and length of structure $L = 1$ cm determine the resolution in MSBVW spectrum in terms of wave number $\Delta k = 2\pi/L \approx 6\,\text{cm}^{-1}$ and frequency $\Delta f = t^{-1} = 1$ MHz. The results shown in Figure 3 and Figure 4 were obtained at attenuation of $\alpha = 10^{-5}$ which is more than by order lower than real losses on YIG. With the value $\alpha = 3 \cdot 10^{-4}$ typical for YIG and selected parameters of micro-magnetic simulation only BR for principal mode can be settled.

4. Conclusion

Thus, this paper outlines the spin pumping with traveling MSBVW waves in a YIG-film magnonic crystal — platinum structure (MC-Pt). It is demonstrated that effectiveness of spin pumping with running MSBVW waves can have a rising resonance at Bragg resonance (BR) frequencies due to growth of the density of states in SW spectrum at the band gap edges. The multimode nature of MSBVW propogation is found to lead to formation of local band gaps. At that, the band gap at BR frequencies of MSBVW principal mode (m = 1) may include the resonances of MSBVW modes with numbers m ≥ 2.

Funding

This study was supported financially by the Russian Science Foundation (Grant 22-19-00500). The work by S.A. Nikitov was performed under the State assignment called „Spintronics“. The work by A. Khitun was partially supported by the National Scientific Fund (NSF) within Project No. 2006290, Program Supervisor — S. Basu,

Dr. Sc. and INTEL corporation (Grant No. 008635, Spin Wave Computing). Project Director — D.E. Nikonov, Dr. Sc.

Conflict of interest

The authors declare that they have no conflict of interest.

References

[1] A. Chumak, V. Vasyuchka, A. Serga, B. Hillebrands. Nature Phys. **11**, 453 (2015). https://doi.org/10.1038/nphys3347
[2] S.A. Nikitov, D.V. Kalyabin, I.V. Lisenkov, A.N. Slavin, Yu.N. Barabanenkov at al. UFN, **185**, 1099 (2015). (in Russian).
[3] S.A. Nikitov, A.R. Safin, D.V. Kalyabin, A.V. Sadovnikov, E.N. Beginin, M.V. Logunov, M.A. Morozova, S.A. Odintsov, S.A. Osokin, A.Yu. Sharaevskaya, Yu. P. Sharaevsky, A.I. Kirilyuk, UFN **190**, 1009 (2020). (in Russian).
[4] V.E. Demidov, S. Urazhdin, G. de Loubens, O. Klein, V. Cros, A. Anane, S.O. Demokritov. Phys. Rep. **673**, 23 (2017). http://dx.doi.org/10.1016/j.physrep.2017.01.001
[5] M. Althammer. J. Phys. D **51**, 313001 (2018); DOI: 10.1088/1361-6463/aaca89
[6] V.E. Demidov, S. Urazhdin, A. Anane, V. Cros, S.O. Demokritov. J. Appl. Phys. **127**, 170901 (2020). https://doi.org/10.1063/5.0007095
[7] A. Brataas, B. van Wees, O. Klein, G. de Loubens, M. Viret. Phys. Rep. **885**, 1 (2020). https://doi.org/10.1016/j.physrep.2020.08.006
[8] Y. Kajiwara, K. Harii, S. Takahashi, J. Ohe, K. Uchida, M. Mizuguchi, H. Umezawa, H. Kawai, K. Ando, K. Takanashi, S. Maekawa, E. Saitoh. Nature **464**, 262 (2010). DOI: 10.1038/nature08876
[9] M. Collet, X. de Milly, O. d'Allivy Kelly, V.V. Naletov, R. Bernard, P. Bortolotti, J. Ben Youssef, V.E. Demidov, S.O. Demokritov, J.L. Prieto, M. Muñoz, V. Cros, A. Anane, G. de Loubens, O. Klein. Nature Commun. **7**, 10377 (2016). https://doi.org/10.1038/ncomms1037720
[10] M. Evelt, V.E. Demidov, V. Bessonov, S.O. Demokritov, J.L. Prieto, M. Muñoz, J. Ben Youssef, V.V. Naletov, G. de Loubens, O. Klein, M. Collet, K. Garcia-Hernandez, P. Bortolotti, V. Cros, A. Anane. Appl. Phys. Lett. **108**, 172406 (2016). https://doi.org/10.1063/1.4948252
[11] K.-I. Uchida, H. Adachi, T. Ota, H. Nakayama, S. Maekawa, E. Saitoh. Appl. Phys. Lett. **97**, 172505 (2010). https://doi.org/10.1063/1.3507386
[12] C.W. Sandweg, Y. Kajiwara, A.V. Chumak, A.A. Serga, V.I. Vasyuchka, M.B. Jungfleisch, E. Saitoh, B. Hillebrands. Phys. Rev. Lett. **106**, 216601 (2011). https://doi.org/10.1103/PhysRevLett.106.216601
[13] H. Kurebayashi, O. Dzyapko, V.E. Demidov, D. Fang, A.J. Ferguson, S.O. Demokritov. Nature Mater. **10**, 660 (2011). https://doi.org/10.1038/NMAT3053
[14] Y. Tserkovnyak, A. Brataas, G.E.W. Bauer. Phys. Rev. Lett. **88**, 117601 (2002). https://doi.org/10.1103/PhysRevLett.88.117601
[15] Z. Qiu, K. Ando, K. Uchida, Y. Kajiwara, R. Takahashi, H. Nakayama, T. An, Y. Fujikawa, E. Saitoh. Appl. Phys. Lett. **103**, 092404 (2013). https://doi.org/10.1063/1.4819460
[16] L.Liu, Y. Li, Y. Liu, T. Feng, J. Xu, X.R. Wang, D. Wu, P. Gao, J. Li. Phys. Rev. B **102**, 014411 (2020). DOI: 10.1103/PhysRevB.102.014411
[17] D. Song, L. Ma, S. Zhou, J. Zhu. Appl. Phys. Lett. **107**, 042401 (2015). https://doi.org/10.1063/1.4927551
[18] E.G. Tveten, A. Brataas, Y. Tserkovnyak. Phys. Rev. B **92**, 180412(R) (2015). https://doi.org/10.1103/PhysRevB.92.180412
[19] L. van Hove. Phys. Rev. **89**, 1189 (1953). https://doi.org/10.1103/PhysRev.89.1189
[20] G. Li, H. Jin, Y. Wei, J. Wang. Phys. Rev. B **106**, 205303 (2022). https://doi.org/10.1103/PhysRevB.106.205303
[21] V. Kalappattil, R. Geng, R. Das, M. Pham, H. Luong, T. Nguyen, A. Popescu, L.M. Woods, M. Klaui, H. Srikanth, M.H. Phan. Mater. Horizons **7**, 1413 (2020). https://doi.org/10.1039/C9MH01498E
[22] L. Wang, Z. Lu, J. Xue, P. Shi, Y. Tian, Y. Chen, S. Yan, L. Bai, M. Harder. Phys. Rev. Appl. **11**, 044060 (2019).
[23] Y.Z. Wang, T.Y. Zhang, J. Dong, P. Chen, G.Q. Yu, C.H. Wan, X.F. Han. Phys. Rev. Lett. **132**, 076701 (2024).
[24] R.W. Damon, J.R. Eshbach. J. Phys. Chem. Solids **19**, 308 (1961). DOI: 10.1016/0022-3697(61)90041-5
[25] M.E. Seleznev, Y.V. Nikulin, Y.V. Khivintsev, S.L. Vysotsky, A.V. Kozhevnikov et al. Zhurnal radioelectroniki 12, (2023). http://jre.cplire.ru/jre/dec23/4/abstract.html (in Russian)
[26] S.L. Vysotsky, Yu.V. Nikulin, G.M. Dudko, V.K. Sakharov, A.V. Kozhevnikov, et all. 2022 Int. Conf. Actual Problems of Electron Devices Engineering (APEDE) — IEEE, **1**, 32 (2022). https://ieeexplore.ieee.org/abstract/document/9912920
[27] A.V. Chumak, A.A. Serga, B. Hillebrands, M.P. Kostylev. Appl. Phys. Lett. **93**, 022508 (2008).
[28] A.V. Chumak, A.A. Serga, S. Wolff, B. Hillebrands, M.P. Kostylev. J. Appl. Phys. **105**, 083906 (2009).
[29] A.V. Chumak, A.A. Serga, S. Wolff, B. Hillebrands, M.P. Kostylev. Appl. Phys. Lett. **94**, 172511 (2009). https://doi.org/10.1063/1.3127227
[30] D. Richardson, B.A. Kalinikos, L.D. Carr, M. Wu. Phys. Rev. Lett. **121**, 107204 (2018). https://doi.org/10.1103/PhysRevLett.121.107204
[31] U.V. Gulyaev, S.A. Nikitov. Dokl. of the Academy of Sciences **380**, 469 (2001). (in Russian).
[32] S.A. Nikitov, Ph. Tailhades, C.S. Tsai, J. Magn. Magn. Mater 236, 320 (2001).
[33] S.L. Vysotsky, S.A. Nikitov, Yu.A. Filimonov. J. Exp. Theor. Phys., **128**, 636 (2005). (in Russian).
[34] M.J. Donahue, D.G. Porter. OOMMF user's guide. Interagency Rep. NIST 6376 (1999).
[35] M. Dvornik, Y. Au, V.V. Kruglyak. In: Magnonics. / Ed. S. Demokritov, A. Slavin. Springer, Berlin (2013). 125.P. 101–115.
[36] V.K. Sakharov, Yu.V. Khivintsev, G.M. Dudko, A.S. Jumaliev, A.V. Kozhevnikov, S.L. Vysotsky, A.I. Stogny, Y.A. Filimonov. FTT **64**, 1255 (2022). (in Russian).

Translated by T.Zorina